ADVANCED FUNCTIONAL MATERIALS
www.afm-journal.de

Materials Views
www.MaterialsViews.com

The Bottom Up Approach is Not Always the Best Processing Method: Dense α-Al_2O_3/$NiAl_2O_4$ Composites

*Nathan J. Taylor, Andrew J. Pottebaum, Veli Uz, and Richard M. Laine**

The bottom up approach suggests that atomic scale mixing should permit optimal control of processing for many types of materials in terms of densification rates, final and average grain sizes; and, thereafter, global properties thereby minimizing processing conditions, capital equipment requirements, and energy consumption. The literature indicates that, to date, this axiom has not been tested although numerous researchers have whole-heartedly adopted the concept. Liquid-feed flame spray pyrolysis (LF-FSP) provides atomically mixed $NiO{\cdot}3Al_2O_3$ nanopowders(30–40 nm average particle size, APS) that are a single phase, spinel solid solution. Sintering 56 ± 1 wt% CIPped pellets to 95 ± 1% theoretical density using two different heating schedules produces α-Al_2O_3/$NiAl_2O_4$ composites with grain sizes of 0.9 ± 0.2 μm. For comparative purposes, ball milled Al_2O_3 are synthesized from both highly atomically-mixed single phase metastable spinel nanopowders and $NiAl_2O_4$ 30–40 nm APS pellets of the same composition with a submicrometer length scale mixing and similar green densities are also sintered to 95 ± 2% TD. In both instances, the same microstructures are realized despite the great difference in length scale of mixing. This contrasts greatly with the expectation that the atomically mixed materials would give finer grain sizes at the same densities and with faster sintering times, suggesting that the bottom up approach is not always valid.

1. Introduction

A long-standing concept in materials processing is that material properties can be improved by starting with better and finer mixing of reactive components.[1–5] Mixing at finer length scales is also thought to provide better control of final microstructural properties, which in turn can lead to better control of macroscopic (global) properties.[6–8] To take full advantage of this bottom-up approach, one can suggest that true atomic scale mixing should provide optimal control of microstructural evolution and compositional control at the finest feature sizes.

In the field of ceramics processing, where the energetics of sintering require extended periods at high temperatures to activate diffusion processes, the bottom-up concept appears to be the best approach to obtaining high quality monoliths with exceptional control of densities and final grain sizes. While the axiomatic bottom-up approach is often applied to the synthesis of nanostructured devices, surprisingly; the effect of the bottom-up approach on the synthesis of bulk materials has yet to be investigated. Applied to composite systems of two or more phases, our expectation was that starting from the bottom-up, the densest composites with the finest grain sizes would obtain from atomically mixed metastable nanopowders.

Liquid-feed flame spray pyrolysis (LF-FSP) involves the combustion of alcohol solutions of simple metalloorganic precursors such as carboxylates, alkoxides, or β-diketonates.[9–12] The resultant metal oxide or mixed-metal oxide nanopowder "soot" is quenched rapidly at rates >1000 °C s^{-1} and collected 1.5 m downstream in electrostatic precipitators at rates of up to 100 g h^{-1}. LF-FSP gas phase particle production has the advantage of producing oxide nanopowders with nearly perfect atomic mixing and access to exact stoichiometries. We have previously synthesized a number of phase pure, metastable spinels with atomic scale elemental mixing at compositions well outside the normally reported phase fields.[9–12] We have also reported the synthesis of fine grained composite materials such as t-ZrO_2-α-Al_2O_3 materials that exhibit enhanced mechanical properties.[13]

Spinels are a class of transition metal oxides with the general structure AB_2O_3. The spinel structure consists of an FCC oxygen sublattice with cations occupying 1/8 the tetrahedral sites and ½ the octahedral sites. In the normal spinel structure, the B^{3+} cations occupy the octahedral sites with the A^{2+} cations occupying the tetrahedral sites. In the inverse spinel structure, the divalent cations occupy the octahedral sites, while the trivalent cations occupy the tetrahedral sites.[14] In addition, many spinels exist with mixed character, leading to the general formula $(A_{1-x}B_x)[A_xB_{2-x}O_4]$ with $(A_{1-x}B_x)$ indicating tetrahedral occupancy and $[A_xB_{2-x}O_4]$ representing octahedral occupancy, where x represents the degree of inversion. The determination of the spinel inversion parameter across many systems has been a common academic exercise.[15]

Taking into account electrostatic interactions, atomic radii, and ligand field effects, Ni is commonly reported to have high octahedral site preference energy (OSPE), driving the formation of inverted spinels.[15] As reported in our previous work on $NiO \cdot 3Al_2O_3$, the presence of a single phase material requires that some Al^{3+} cations occupy octahedral sites, leading to a

N. J. Taylor, A. J. Pottebaum, V. Uz, Prof. R. M. Laine
Department of Materials Science and Engineering
University of Michigan
Ann Arbor, MI 48109-2136
E-mail: talsdad@umich.edu

DOI: 10.1002/adfm.201302845

mixed spinel. In addition, δ-Al_2O_3 is commonly formed in gas-phase Al_2O_3 nanopowder syntheses.[16] δ-Al_2O_3 is normally described as a defect spinel structure, where 8/3 Al tetrahedral vacancies account for spinel cation vacancies.[17] Al_2O_3 rich spinel solid solutions have been well characterized in the MgO–Al_2O_3 system, and the corresponding defect reaction can be shown in:[18,19]

$$4Al_2O_3 \rightarrow V_{Ni}^{+}2Al_{Ni}^{\cdot} + 6Al_{Al}^{X} + 12O_O^X \quad (1)$$

Nickel aluminate spinel materials have been explored in considerable detail for multiple reasons. For example, the spinel material is used as a pigment.[20] It is also used as a electrode material in high temperature fuel cells because of its unusual conductivity.[21–23] It is also used as a catalyst or a precatayst for steam reforming.[24,25] $NiAl_2O_4$–Al_2O_3 composites may also have application as a structural ceramic material.[26]

The introduction of excess alumina into the nickel aluminate spinel does not significantly change the color of the resulting nanopowder, consequently one might envision using the reduced nickel content materials as replacement pigments, assuming that there is no change in properties when these pigments are used in ceramic glazes for example. As electrode materials, there is interest in making dense materials that retain their mechanical properties, their electrical properties and that also offer thermal stability after continued use in SOFC environments.[22] Finally, steam reforming catalysts are usually nickel on alumina and normally activity will be related to the nickel particle size where smaller particle sizes equal higher catalytic activities.[27] The materials we produce below are dense ceramics but they are oxides and could be reduced for catalytic activity. One can assume that finer grain sizes will lead to smaller Ni particles on reduction that could in principle lead to higher catalytic activity. In addition, the reduction process will produce Ni particles in or on an alumina matrix and will create porosity. While this is not the objective of the current manuscript; all of the above applications will benefit from an understanding of the thermal behavior of the materials produced by the two processing approaches explored here.

2. Results and Discussion

The objectives of the work discussed here are to explore the potential utility of using atomically mixed metastable $NiO \cdot 3Al_2O_3$ nanopowders (APSs 30–40 nm) as a starting point for processing ceramic-ceramic composites with optimal control of the densification process, final average grain sizes and in principle with optimal macroscopic properties. This approach is an effort to test the efficacy of the bottom up approach. To ensure a fair comparison with other processing approaches, we also performed a side-by-side comparison using equivalent composition ball-milled mixtures of δ-Al_2O_3 and $NiAl_2O_4$ (APSs 30–40 nm for both). In the latter case, ball milling is anticipated to lead to compositional homogeneity only at submicrometer length scales. Thus, there was considerable disparity in the homogeneity length scales in the green state.

We begin by discussing the synthesis and characterization of the powders used in the study through BET surface area analysis, SEM, TEM, XRD, and DRIFTS. Thereafter we discuss the results of sintering studies and the final microstructures as shown by SEM of composites prepared from atomically mixed $NiO \cdot 3Al_2O_3$ as well as ball-milled two-component mixtures with the same composition.

Table 1. BET SSAs and derived APSs for nanopowders used in this study.

Powder	Density [g cm^{-3}]	SSA [m^2 g^{-1}]	APS [nm]
$NiO{\cdot}3Al_2O_3$	4.16	43	34
$NiAl_2O_4$	4.49	42	31
Nanotek Al_2O_3	3.6	30	56

2.1. BET Surface Area Analysis

Specific surface areas (SSAs) for all powders used in this study are listed in **Table 1**. No microporosity was detected nor is microporosity common in LF-FSP nanopowders. Average particle sizes (APSs) were calculated from the SSAs using the theoretical densities and assuming spherical powder morphologies. All SSAs are ±1 m^2 g^{-1}, which give APSs within ±2 nm. SSAs were repeatable across different production runs within ±3 m^2 g^{-1}.

2.2. Scanning Electron Microscopy

SEM was performed on all as-produced powders to establish overall particle morphology and qualitatively investigate the overall particle size distribution. **Figure 1** shows a representative SEM image of as-produced $NiO \cdot 3Al_2O_3$. All particles show similar spherical morphology, and appear agglomerated. A few >100 nm particles are present, but the majority appear to be

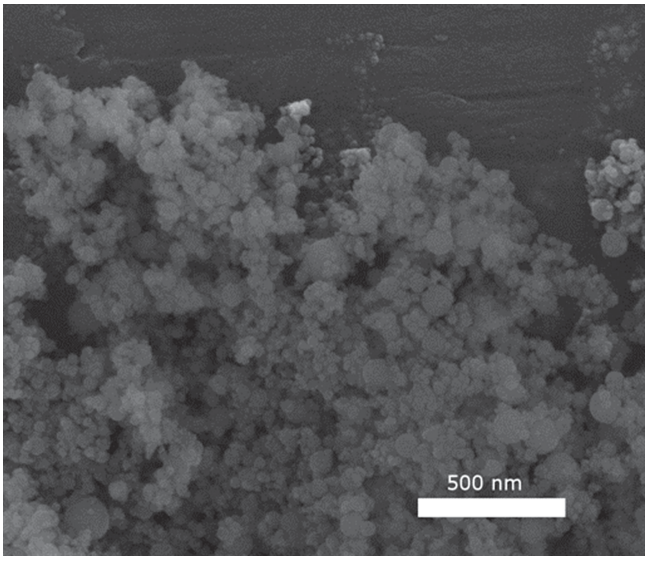

Figure 1. Representative scanning electron micrograph of as-produced $NiO{\cdot}3Al_2O_3$ nanopowder. Some larger particles are present but the majority agree with BET derived APSs.

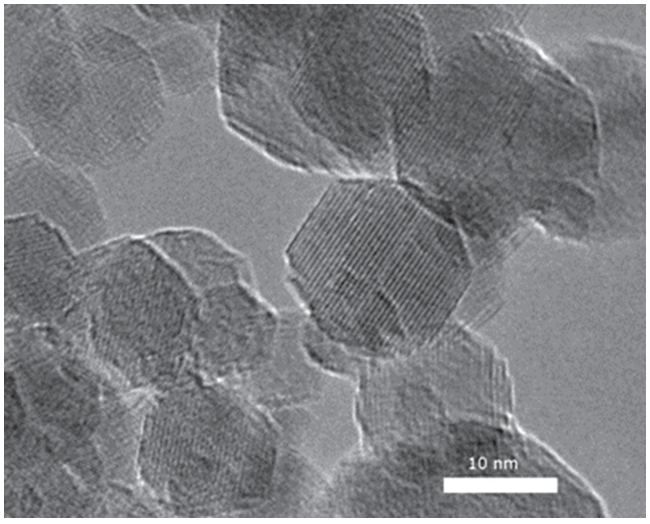

Figure 2. TEM image showing $NiO{\cdot}3Al_2O_3$. Single crystal particles are faceted and agglomerated. The majority of particles are unaggregated.

<50 nm, which correlates well with BET derived particle sizes. No fraction of large >1 μm particles were observed by SEM.

2.3. Transmission Electron Microscopy

TEM provides more information including particle morphology and degree of aggregation. **Figure 2** provides a representative TEM image of as-produced $NiO \cdot 3Al_2O_3$. TEM indicates most particles are agglomerated, highly faceted, single crystals. Some aggregates are observed by TEM, but this represents only a small fraction of the particles.

2.4. X-Ray Diffraction

As seen in **Figure 3**, XRD indicates as-produced $NiO \cdot 3Al_2O_3$ is a single phase material. δ-Al_2O_3 is isostructural with the spinel structure allowing for ready formation of solid solutions.[17] Calculations provide a lattice constant for as-produced $NiO \cdot 3Al_2O_3$ at a point 53% along the Al_2O_3-$NiAl_2O_4$ tie line (see experimental section) in keeping with Vegard's law, supporting the classification of the atomically mixed, metastable spinel as a δ-Al_2O_3/$NiAl_2O_4$ solid solution.

XRDs of the as-produced stoichiometric $NiAl_2O_4$ powder find spinel as the primary phase, with some (<5 wt%) bunsenite (NiO) (see Supporting Information, Figure S1). The presence of bunsenite remains unexplained, but may relate to the kinetics of the quenching process. However, XRDs of stoichiometric $NiAl_2O_4$ sintered to high temperature (1400 °C) did not indicate any extraneous phases, so overall, the composition seems to be correct.

On heating $NiO \cdot 3Al_2O_3$ powders to the phase transformation temperature for α-Al_2O_3, 1150 °C, α-Al_2O_3 nucleates from Al_2O_3 rich spinel.[17] **Figure 4** shows TGA-DTA, indicating a phase transformation temperature of 1205 °C. This temperature lies above some more common α-transformation temperatures, and ≈45 °C less than the DTA exotherm corresponding to α-Al_2O_3

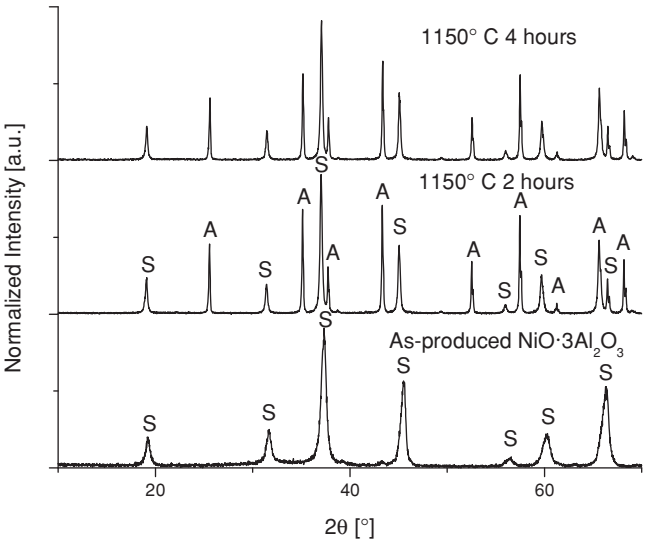

Figure 3. XRD spectra for as-produced $NiO{\cdot}3Al_2O_3$ as well as samples heated for two and four hours at 1150 °C. (A = α-Al_2O_3, S = $NiAl_2O_4$ spinel) The as-produced sample is single phase corresponding to $NiAl_2O_4$. The calcined samples indicate segregation of α-Al_2O_3.

transformation for Nanotek Al_2O_3 (SI, Figure S2). The lower exotherm is likely an effect of Ni doping, which has been shown to reduce the α-transformation temperature.[29] TGA mass loss above 1200 °C can be attributed to the slight volatility of NiO.[30] Figure 3 presents XRDs for as-produced $NiO \cdot 3Al_2O_3$ powder and samples heated to 1150 °C for 2 and 4 h. The only phase present for as-produced $NiO \cdot 3Al_2O_3$ is identical to $NiAl_2O_4$ spinel (PDF: 01-071-0963). After heating to 1150 °C, α-Al_2O_3 (PDF: 01-078-2427) appears. Further heating does not increase the α-Al_2O_3 content indicating that 2 h/1150 °C is sufficient for full phase segregation. XRD shows Nanotek is a mixed transition-Al_2O_3, consisting of δ, δ^*, and θ-Al_2O_3.

The **Figure 5** SEM shows a fracture surface after heating as-produced $NiO \cdot 3Al_2O_3$ pellet to 1150 °C/4 h/air. Large islands >200 nm of α-Al_2O_3 have formed within the spinel (now primarily $NiAl_2O_4$) matrix, which undergoes little grain growth. These islands were confirmed to be α-Al_2O_3 by EDS

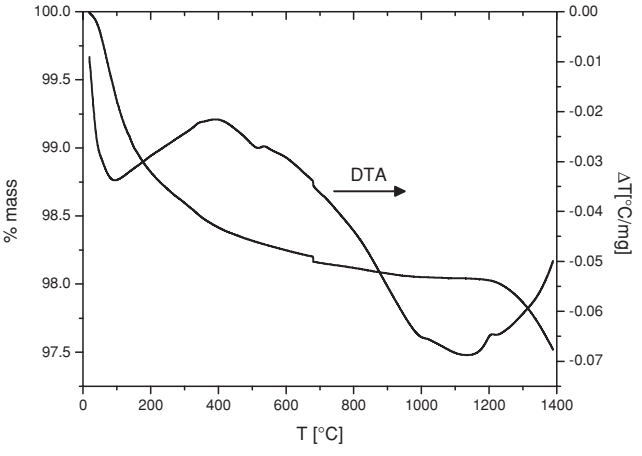

Figure 4. TGA/DTA traces for as-produced $NiO{\cdot}3Al_2O_3$.

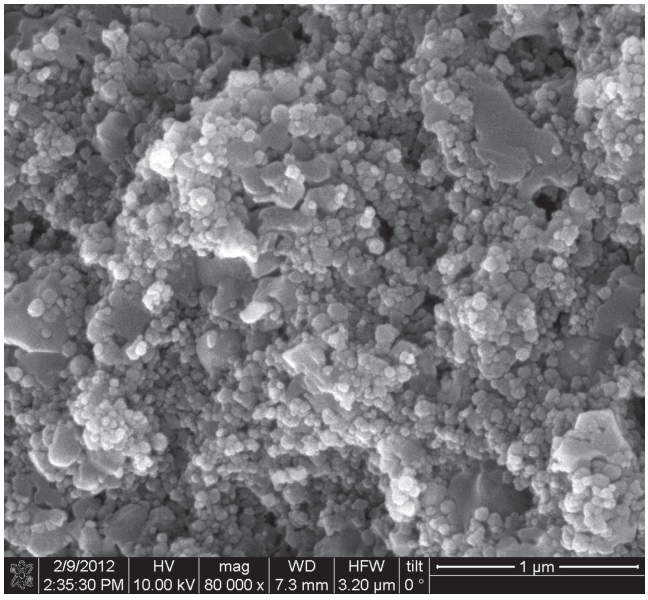

Figure 5. SEM image of demixed sample heated to 1150 °C for 2 h/air. The large grains are α-Al_2O_3, while the spinel particles have barely coarsened.

and Scherrer line broadening. It is important to note that no transition-Al_2O_3 phases were observed prior to α-Al_2O_3 segregation. The transformation sequence of the defect spinel, γ-Al_2O_3, involves transformation through both the δ and θ phases prior to transformation to the α-Al_2O_3 phase.[17] This observation suggests no segregation of Al_2O_3 exists prior to nucleation of the α-Al_2O_3 phase, which means the driving force for Al_2O_3 segregation appears to be α-Al_2O_3 nucleation.

2.5. DRIFTS

Spectra for as-produced $NiO \cdot 3Al_2O_3$ as well as a sample heated to 1150 °C/2 h/air/10 °C min^{-1}, LF-FSP $NiAl_2O_4$, and Nanotek Al_2O_3 are presented in **Figure 6**. The 1800–4000 cm^{-1} region is magnified 10x. The broad νOH 3700–2500 cm^{-1} band corresponds to both physi- and chemi-sorbed water and is typical for LF-FSP nanopowders. These species are not seen in the 1150 °C $NiO \cdot 3Al_2O_3$ FTIR. The 1000–400 cm^{-1} region exhibits νM-O absorptions bands with a νNi-O peak at 500 cm^{-1}.[1] Peaks near 600 and 800 cm^{-1} correspond to octahedrally and tetrahedrally coordinated νAl-O respectively, and are present in all samples.[26]

The observation of mixed octahedral/tetrahedral νAl-O bands in as-produced material is indicative of a highly disordered spinel structure (elemental mixing at atomic length scales). Peak narrowing coincident with increased relative intensity of the 600 cm^{-1} with respect to the 800 cm^{-1} peak in the 1150 °C material is a consequence of α-Al_2O_3 nucleation as it contains only AlO_6 octahedra. Nanotek Al_2O_3 shows peaks at 600 and 800 cm^{-1}, characteristic for νAl-O octahedral and tetrahedral environments, respectively, along with a broad νOH peak.[31] Figure 4 provides a TGA/DTA showing a 1.9 wt% mass loss at 1100 °C, consistent with the loss of chemisorbed water and CO_2 as observed in the DRIFT spectra. TGA/DTA traces of $NiAl_2O_4$ and Nanotek Al_2O_3 (Figure S2) show similar mass losses <3 wt% corresponding to elimination of surface hydroxyls and traces of CO_2.

Drawing on the phase separation behavior exhibited by the metastable particles, we began to process $NiO \cdot 3Al_2O_3$ into compacts to produce α-Al_2O_3/$NiAl_2O_4$ composite materials. The exact composition was also matched by ball milling of stoichiometric LF-FSP $NiAl_2O_4$ nanopowder with commercial Nanotek Al_2O_3 nanopowder to produce a $NiO \cdot 3Al_2O_3$ composition. All samples were subject to the same processing conditions and all samples reached a minimum post-CIP density of 55 wt% of theory (TD).

Two sintering schedules were investigated for both metastable $NiO \cdot 3Al_2O_3$ and ball-milled $NiAl_2O_4$ + Al_2O_3. The first schedule (H1) was a 10 h isothermal hold at 1400 °C, which produced samples at least 95% TD, which is assumed to be sufficient for HIPing to 100% TD. Ramp rates are discussed in the experimental section above.

To investigate the role of phase transformation on sintering behavior and final microstructure, a second heating schedule (H2) was investigated. The second heating schedule was designed to fully demix the samples prior to densification and minimize grain growth through lower temperature sintering. Further isothermal sintering was performed until densification

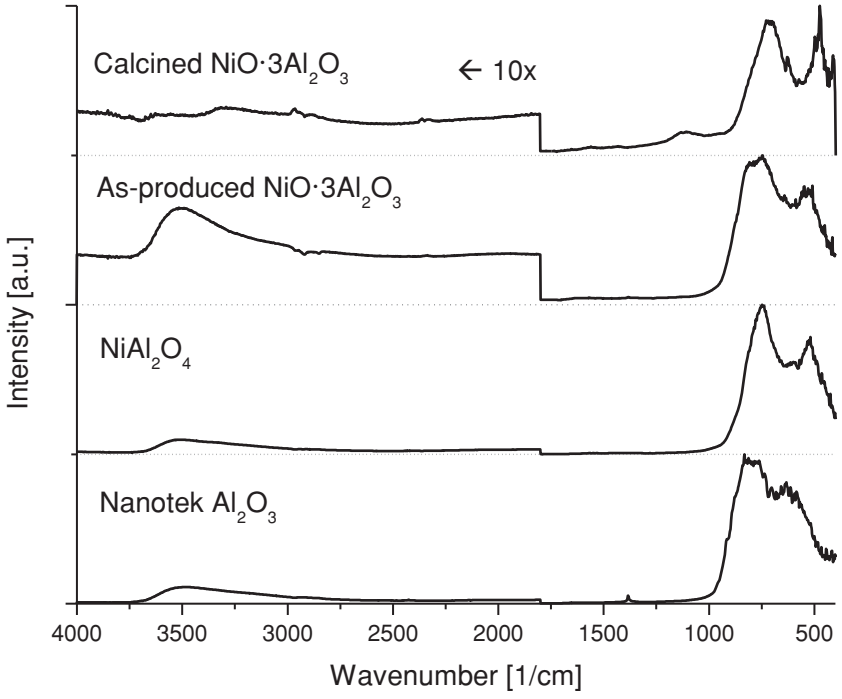

Figure 6. DRIFTS spectra for as-produced $NiO{\cdot}3Al_2O_3$, $NiO{\cdot}3Al_2O_3$ calcined for 2 h/1150 °C/air, LF-FSP stoichiometric $NiAl_2O_4$, and Nanotek Al_2O_3.

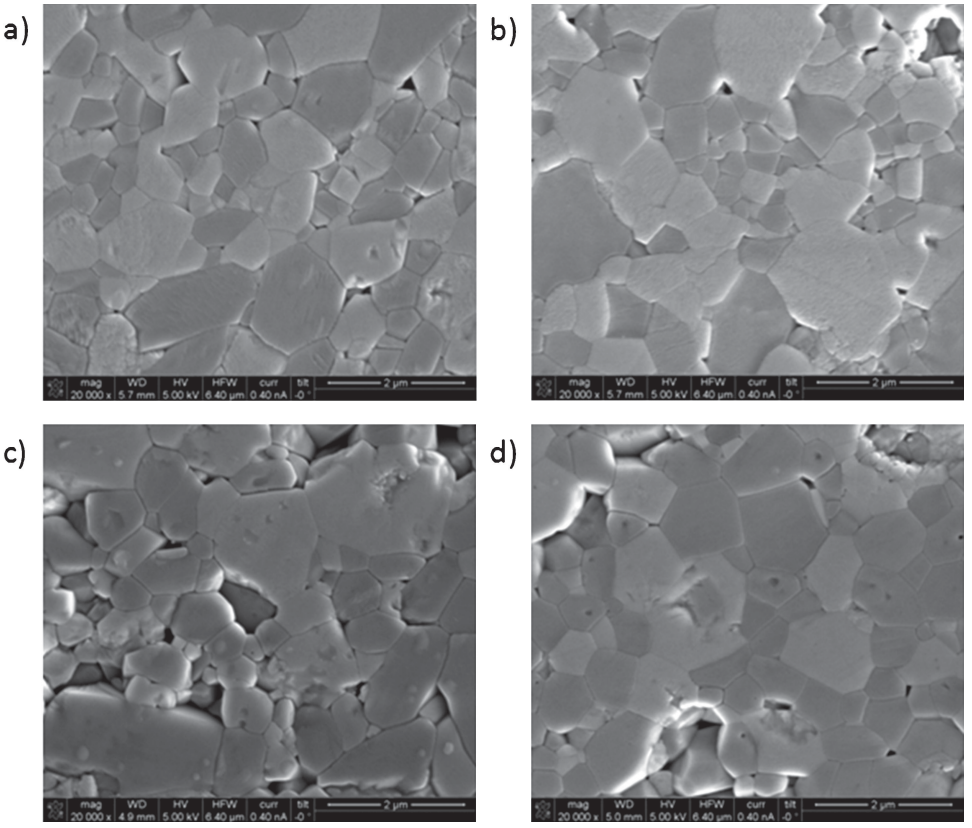

Figure 7. SEM images of polished pellet surfaces: a) $NiO{\cdot}3Al_2O_3$ (H1), b) $NiO{\cdot}3Al_2O_3$ (H1), c) milled $NiAl_2O_4 + Al_2O_3$ (H1), d) milled $NiAl_2O_4 + Al_2O_3$ (H2).

stopped, at which point the sintering temperature was raised. The second heating schedule was at 1150 °C/4 h, 1300 °C/8 h, and 1400 °C/4 h, which also produced samples at least 95 wt% TD. The sintering studies were performed in dry N_2, vacuum, and air, and no differences in densification or grain sizes were observed. Diffusion in Al_2O_3 rich spinels is dominated by cation-vacancy movement, so low pO_2 should have no effect on sintering behavior.[18]

Figure 7 provides SEM images of polished pellet cross sections. **Table 2** records post-CIP green densities, final densities, and average grain sizes (AGSs) as determined by the lineal intercept. AGSs for all sintered samples were <1 μm at densities greater than 95% TD.

Extensive SEM investigation of the polished samples found no noticeable differences in final microstructure. This observation is significant, given the length scales of initial phase separation in the starting materials. As noted above, while the $NiO \cdot 3Al_2O_3$ powders were atomically mixed, the ball-milled $NiAl_2O_4$+ Al_2O_3 samples were mixed at significantly longer length scales.

Given that the individual APSs are 30–40 nm, we do not believe that it is possible by simply ball milling to achieve uniform mixing at length scales finer than submicrometer.

In an effort to determine if there were subtle differences between the two materials during densification, we undertook dilatometry studies. As seen Figures S4 and S5 there are no obvious differences in the densification temperatures or processes between the two approaches. This result alone is quite surprising but further studies remain to explore this issue and will be presented at a later date.

3. Conclusions

Dense α-$Al_2O_3/NiAl_2O_4$ nanocomposites were prepared from both atomically mixed single phase $NiO \cdot 3Al_2O_3$ nanopowders and ball milled mixtures of $NiAl_2O_4$ and Al_2O_3 nanopowders produced by LF-FSP. Processing and sintering $NiO \cdot 3Al_2O_3$ gave composites at 95 %TD gave final microstructures, average grain sizes, and densification behavior that was identical to that

Table 2. Sintering conditions and final densities with average grain sizes for both composites.

Composition	TD (g cm^{-3})	CIP density %TD	Heating schedule	Final density %TD	Average grain size (nm)
$NiO{\cdot}3Al_2O_3$	4.16	55% ± 0.8%	1400 °C – 10 h	95% ± 0.9%	910 ± 170
$NiAl_2O_4 + Al_2O_3$	4.16	57% ±1.2%	1400 °C – 10 h	96% ± 0.8%	870 ± 208

of $NiO \cdot 3Al_2O_3$ composites produced through ball milling of nanopowders. The resultant composites have a range of possible applications, but this study represents a look at the synthesis and processing pathway needed to reach the finest, most uniform microstructure.

The bottom-up approach, as it stands, is one of the cornerstones of new material development; yet the synthesis of bulk materials from the bottom up is a underdeveloped field. In this work, we have shown one example of the synthesis of a bulk composite from the bottom-up that does not provide an advantage over a more traditional processing approach. The attractive properties of highly-dispersed, fine grained ceramic composite materials will continue to drive investigation in this field, and more complete studies of phase evolution and densification behavior may outweigh attention to highly atomically-mixed starting materials.

A related paper on processing atomically mixed $Y_3Al_5O_{12}$ vs ball milled 3:5 mixtures of Y_2O_3 and Al_2O_3 also provides results that greatly contrast with the bottom-up axiom.[32]

In future papers, we will discuss LF-FSP studies of analogous spinel composite systems, including $MgAl_2O_4/Al_2O_4$ and $CoAl_2O_4/Al_2O_4$ as well as binary $Y_3Al_5O_{12}/Al_2O_3$, $Y_3Al_5O_{12}/MgAl_2O_4$, and ternary $Y_3Al_5O_{12}/Al_2O_3/ZrO_2$ composites.[33]

4. Experimental Section

Precursors: Alumatrane was synthesized as described elsewhere.[28] Anhydrous ethanol was purchased from Decon Labs (King of Prussia, PA). Nickel acetate was purchased from Sigma Aldrich (Milwaukee, WI) and used as received. Nanotek Al_2O_3 (Nanophase Technologies Corporation, Romeoville, IL) was received as a gift.

LF-FSP: Precursors were dissolved in ethanol solutions at less than 3 wt% ceramic loading. Solutions were aerosolized with 40 ml/min of extra dry O_2 at 80 psi. 150 mL min^{-1} of shield O_2 was injected at 80 psi. Powders were collected in electrostatic precipitators with a 10 kV DC pseudopotential.

Powder Processing: Approximately 30 g of as-produced $NiO{\cdot}3Al_2O_3$ LF-FSP powder was added to 350 mL of ethanol, with 2 wt% bicine as a dispersant and ball milled for 24 h with 3 mm 99% pure Al_2O_3 media. The suspension was ultrasonicated for 20 min using a Vibracell VC-505 ultrasonic horn (Sonics & Materials, Newtown, CT) at 100 W of power. After a 24 h settling period, the supernatant was decanted and dried. The dried powders were sieved through a 75 μm polymer mesh and dispersed in an ethanol solution with 4 wt % PEG 3400 as binder. The dried powders were sieved through 20 μm polymer mesh, uniaxially pressed at 14 MPa, and CIP'd to 200 MPa. Ball milled $NiO{\cdot}3Al_2O_3$ composites were processed under identical conditions, except undergoing ultrasonication and settling prior to ball milling to ensure stoichiometry was maintained.

Burnout and Sintering: Pellets were burned out at 3 °C min^{-1} to 500 °C for 4 h in dry O_2 at 50 mL min^{-1}. Pellets were sintered in a MTI GSL-1600X (MTI Corp., Richmond, CA) tube furnace under flowing dry air at 50 mL min^{-1}. All sintering ramp rates were 10 °C min^{-1} below 1100 °C, and 5 °C min^{-1} above 1100 °C.

X-ray Diffraction (XRD): X-ray diffraction was performed on a high-intensity Rigaku rotating anode at 40 kV and 100 mA (Rigaku USA, The Woodlands, TX). Sample scans were taken from 10–70° 2θ with 0.02° intervals and scanned at a rate of 2.0° 2θ min^{-1}. X-ray patterns were analyzed using JADE 10.0. Vegard's law calculations were performed using an internal Si (111) standard. The lattice constant calculated from the (400) peak was 0.7980, and was compared to a δ-Al_2O_3 lattice constant of 0.7900 nm and a $NiAl_2O_4$ lattice constant of 0.8050 nm.

Scanning Electron Microscopy (SEM): SEM was performed using a FEI Nova Nanolab dualbeam SEM/FIB (FEI Corporation, Hillsboro, OR) equipped with a Schottky FEG. Powders were dropped onto conductive copper tape on a sample stub. Samples were polished using normal laboratory techniques.

Transmission Electron Microscopy (TEM): TEM was performed on a JEOL 3011 HREM (JEOL Ltd., Tokyo, Japan) at 300 kV. Powders were dispersed in ethanol and wicked through a holey carbon grid.

Surface Area Analysis: SSA's were obtained on a Micromeritics ASAP 2020 sorption analyzer (Norcross, GA). Samples were degassed for 8 h at 400 °C. Analysis was conducted on ≈200 mg samples at 77 K with N_2 adsorbate gas. SSA's were calculated using an 11 point BET method with relative pressures from 0.05–0.35.

Thermogravimetric Analysis-Differential Thermal Analysis (TGA-DTA): Simultaneous TGA-DTA was performed on a Q600 TGA-DTA instrument (TA Instruments, Inc., New Castle, DE). Measurements were taken under 60 mL min^{-1} of compressed extra dry air. Samples (20–40 mg) were pressed in a 3 mm die and placed in an alumina sample pan. The reference pan was alumina. Samples were heated at 10 °C min^{-1} to 1400 °C.

Diffuse Reflectance Infrared Fourier Transform Spectroscopy (DRIFTS): DRIFTS spectra were recorded on a ThermoScientific Nicolet 6700 FTIR spectrometer (ThermoScientific, Waltham, MA). Samples were prepared by grinding 5 mg of sample in 400 mg of optical grade KBr (International Crystal Laboratories, Garfield, NJ). Spectra were taken from 4000–400 cm^{-1} with a resolution of ±4 cm^{-1} with an average of 60 scans. The sample chamber was continuously flushed with N_2 to minimize CO_2 adsorption. New blank KBr reference samples were run every five samples.

Dilatometry: Dilatometry was run using a Theta Industries Dilatatronic II (Port Washington, NY) with a LVDT single push-rod loading dilatometry setup. Data were collected with a LabView progam. Square samples were sectioned from 14.7 mm diameter pellets formed as described above. Constant heating rate experiments were conducted with a heating rate of 10 °C min^{-1} to 1500 °C in static air.

Supporting Information

Supporting Information is available from the Wiley Online Library or from the author.

Acknowledgements

The authors gratefully acknowledge the support of the NSF through DMR 1105361.

Received: August 13, 2013
Revised: December 22, 2013
Published online: February 12, 2014

[1] C. M. Lieber, *MRS Bulletin.* **2003**, *28*, 486.
[2] L. Zhi, K. Mullen, *J. Mater. Chem.* **2008**, *18*, 1472.
[3] R. Murugavel, H. G. Walawalkar, M. Dan, H. W. Roesky, C. N. R. Rao, *Acc. Chem. Res.* **2004**, *37*, 763.
[4] L. G. Hubert-Pfalzgraf, *J. Mater. Chem.* **2004**, *14*, 3113.
[5] W. Lu, C. M. Lieber, *Nat. Mater.* **2007**, *6*, 841.
[6] J. Binner, B. Vaidhyanathan, *J. Eur. Ceram. Soc.* **2008**, *28*, 1329.
[7] R. Ramaseshan, S. Sundarrajan, R. Jose, S. Ramakrishna, *J. App. Phys.* **2007**, *102*, 111101.
[8] S. Komarneni, *J. Mater. Chem.* **1992**, *2*, 1219.
[9] J. A. Azurdia, J. Marchal, P. Shea, H. Sun, X. Q. Pan, R. M. Laine, *Chem. Mater.* **2006**, *18*, 731.
[10] T. R. Hinklin, R. M. Laine, *Chem. Mater.* **2008**, *20*, 553.
[11] J. Azurdia, J. Marchal, R. M. Laine, *J. Am. Ceram. Soc.* **2006**, *89*, 2749.

[12] T. R. HinklinJ. A. Azurdia, M. Kim, J. C. Marchal, S. Kumar, R. M. Laine, *Adv. Mater.* **2008**, *20*, 1373.
[13] M. Kim, R. M. Laine, *J. Am. Ceram. Soc.* **2010**, *93*, 709.
[14] R. J. Hill, J. R. Craig, G. V. Gibbs, *Phys. Chem. Mater.* **1979**, *4*, 3.
[15] K. Mocala, A. Navrotsky, *J. Am. Ceram. Soc.* **1989**, *17*, 826.
[16] T. Hinklin, B. Toury, C. Gervais, F. Babonneau, J. J. Gisalon, R. W. Morton, R. M. Laine, *Chem. Mater.* **2004**, *16*, 21.
[17] I. Levin, D. Brandon, *J. Am. Ceram. Soc.* **1998**, *81*, 1995.
[18] Y. Okuyama, N. Kurita, N. Fukatsu, *Solid State Ionics* **2006**, *177*, 59.
[19] C.-J. Ting, H.-Y. Lu, *J. Am. Ceram. Soc.* **1999**, *82*, 841.
[20] N. M. Deraz, *I. J. Electrochem. Sci.* **2013**, *8*, 5203.
[21] Y. S. Han, J. B. Li, X. S. Ning, B. Chi, *J. Am. Ceram. Soc.* **2005**, *88*, 3455.
[22] S. Kurien, J. Mathew, S. Sebastian, S. N. Potty, K. C. George, *Mater. Chem. Phys.* **2006**, *98*, 470.
[23] A. Reyes-Rojas, H. E. Esparza-Ponce, J. Reyes-Gasga, *J. Phys.: Condens. Matter* **2006**, *18*, 4685.
[24] J. R. H. Ross, M. C. F. Steel, A. Zeini-Isfahani, *J. Catal.* **1978**, *52*, 280.
[25] C. Otero Areán, M. Peñarroya Mentruit, A. J. López López, J. B. Parra, *Colloids Surf. A* **2001**, *180*, 253.
[26] D.-K. Kim, W. M. Kriven, *J. Am. Ceram. Soc.* **2008**, *91*, 784.
[27] B. W. Hoffer, A. Dick van Langeveld, J.-P. Janssens, R. L. C. Bonné, C. M. Lok, J. A. Moulijn, *J. Catal.* **2000**, *192*, 432.
[28] R. Baranwal, M. P. Villar, R. Garcia, R. M. Laine, *J. Am. Ceram. Soc.* **2001**, *84*, 951.
[29] M. Ozawa, O. Kato, S. Suzuki, Y. Hattori, M. Yamamura, *J. Mater. Sci. Lett.* **1996**, *15*, 564.
[30] G. de Roos, J. M. Fluit, J. H. W. de Wit, J. W. Gues, *Surf. and Interf. Analysis* **1981**, *3*, 221.
[31] P. Tarte, *Spectrochim. Acta.* **1967**, *23A*, 2127.
[32] N. J. Taylor, R. M. Laine, *Adv. Funct. Mater.* **2013**, DOI: 10.1002/adfm.201301290.
[33] N. J. Taylor, A. J. Pottebaum, V. Uz, R. M. Laine, unpublished.